frontiers | Frontiers in Soft Matter

TYPE Original Research
PUBLISHED 02 November 2022
DOI 10.3389/frsfm.2022.1054658

OPEN ACCESS

EDITED BY
Lingxiang Jiang,
South China University of Technology, China

REVIEWED BY
Yan Qiao,
Institute of Chemistry (CAS), China
Liangfei Tian,
Zhejiang University, China
Yaxun Fan,
Institute of Chemistry (CAS), China

*CORRESPONDENCE
Dehai Liang,
dliang@pku.edu.cn

SPECIALTY SECTION
This article was submitted to Self-Assembly and Self-Organisation, a section of the journal Frontiers in Soft Matter

RECEIVED 27 September 2022
ACCEPTED 17 October 2022
PUBLISHED 02 November 2022

CITATION
Chen J, Liu Z, Li Y, Bai Q, Li Y and Liang D (2022), Coacervation of biopolymers on muscovite surface.
Front. Soft. Matter 2:1054658.
doi: 10.3389/frsfm.2022.1054658

Coacervation of biopolymers on muscovite surface

Jiaxin Chen[1], Zhijun Liu[1], Yanzhang Li[2], Qingwen Bai[1], Yan Li[2] and Dehai Liang[1]*

[1]Beijing National Laboratory for Molecular Sciences, and the Key Laboratory of Polymer Chemistry and Physics of the Ministry of Education, College of Chemistry and Molecular Engineering, Peking University, Beijing, China, [2]Beijing Key Laboratory of Mineral Environmental Function, and the Key Laboratory of Orogenic Belts and Crustal Evolution, School of Earth and Space Science, Peking University, Beijing, China

The first life was believed to emerge in the early Earth *via* a process involving synthesis of organic compounds and formation of protocells. However, it is still a puzzle how the protocell with hierarchal structure and desirable functions was spontaneously generated in the non-living environment composed of mainly water and minerals. In this work, using muscovite as an example of minerals, we systemically studied the coacervation of poly (*L*-lysine) (PLL), quaternized dextran (Q-dextran), and single-stranded oligonucleotide (ss-oligo) on muscovite surface at varying mixing orders. Only when Q-dextran firstly interacts with muscovite surface to form a coating layer, followed by the addition of ss-oligo and PLL, the formed coacervates exhibit distinct and versatile morphologies, including spherical PLL/ss-oligo droplets on the surface, floating PLL/ss-oligo droplets above the Q-dextran/ss-oligo blanket, and PLL/ss-oligo islands surrounded by the Q-dextran/ss-oligo sea. The kinetic pathways to the resulting morphologies are specific in each case. There results suggest that polysaccharide was probably the first biopolymer accumulated on the mineral surface in early Earth. The sugar coating provided a "nest" for protein/peptide and DNA/RNA to from sub-compartments and to further develop advanced functions.

KEYWORDS

origin of life, protocell, coacervate, multiphase, minerals

Introduction

Coacervates are usually formed by oppositely charged polyelectrolytes *via* liquid-liquid phase separations (LLPS) (Sing and Perry, 2020; Rumyantsev et al., 2021). It has been demonstrated that most of the charged biopolymers, such as DNA/RNA, peptides, proteins, lipids, and polysaccharides, are able to form coacervates of varying morphologies and properties (Kruif et al., 2005; Turgeon et al., 2007; Koga et al., 2011; Wang and Wang, 2014; Croguennec et al., 2017; Zhao and Wang, 2017). The formed coacervates are able to enrich molecules, catalyze reactions, and exchange materials with the external environment (Koga et al., 2011; Williams et al., 2012; Black et al., 2014; Tang et al., 2014; Martin et al., 2016; Nakashima et al., 2019; Poudyal et al., 2019). More importantly, the coacervates share the same formation mechanism as the P-granules, Cajal bodies, and

other membraneless organelles found in living cells (Brangwynne et al., 2009; Brangwynne, 2013; Hyman et al., 2014; Feric et al., 2016; Saha et al., 2016; Jiang et al., 2017; Nakagawa et al., 2018; Gomes and Shorter, 2019; Sawyer et al., 2019). Therefore, coacervates have been widely applied as membraneless protocell models to explore the origin of life in early Earth (Douliez et al., 2017; Kumar et al., 2018; Alberti et al., 2019; Abbas et al., 2021; Ghosh et al., 2021; van Haren et al., 2021; Yewdall et al., 2021). With a proper combination of the internal components and the external stimuli, coacervate protocells have achieved many living features, like division, evolution, and metabolism (Dzieciol and Mann, 2012; Zwicker et al., 2016; Nakashima et al., 2018; Spoelstra et al., 2019; Chen et al., 2020).

It is generally accepted that the life was emerged from the non-living environment in the prebiotic Earth (Kee and Monnard, 2016; Sahai et al., 2016). The non-living environment in early Earth mainly consists of water, rocks (minerals), and air (Dalai et al., 2016). Life was supposed to originate in aqueous environment, in which process minerals played key roles (Bernal, 1951; Wächtershäuser, 1992; Pontes-Buarque et al., 2000; Franchi and Gallori, 2005; Gomez et al., 2007; Wächtershäuser, 2007; Xu et al., 2013; Sand and Jelavić, 2018; Ertem, 2021). Growing evidences have demonstrated that the mineral surface is able to concentrate organic molecules, catalyze a variety of reactions, and even serve as reactant (Lahav and Chang, 1976; Ertem and Ferris, 1996; Ferris et al., 1996; Hazen et al., 2001; Ferris, 2002; Zhu et al., 2002; Huang and Ferris, 2003; Miyakawa and Ferris, 2003; Hanczyc et al., 2007; Li et al., 2009; Kawamura et al., 2011; Martra et al., 2014; Liao et al., 2016; Dalai and Sahai, 2019). However, it is still a puzzle how the biopolymers assemble into protocell with hierarchal structure and desirable functions in an aqueous environment in the presence of minerals. Most of the biopolymers are soluble in water. Even though the mixing of the oppositely charged polymers at elevated concentrations is able to generate coacervate droplets *via* LLPS, it is difficult to modulate the structure and properties of the coacervate as LLPS is a spontaneous process. Accumulation of enough biopolymers without hydrolysis is also a limiting step.

The mineral surfaces offer rich opportunities for concentration of biopolymers and possibly their organization into protocells of desirable structures. More than 400 minerals are reported to exist before the origin of life in early Earth (Hazen, 2013). The specific chemical component and the lattice structure render each mineral surface unique physicochemical properties, such as charge, hydrophobicity, functional groups, and dynamic response to environmental conditions like pH, temperature, and ionic strength (Sowerby et al., 2001; Sverjensky, 2005; Sverjensky and Fukushi, 2006; Jonsson et al., 2009). Therefore, a chosen mineral surface should be able selectively absorb the biopolymers *via* attractive interactions, and trigger the formation of protocells if the combination of biopolymers is appropriate and they are mixed in correct order (Hazen et al., 2001; Zaia, 2004; Gan et al., 2009). More importantly, the relationship between the property of the protocell and the mixing order of biopolymers should shed light on the procedure of life's emergence in chosen non-living environment. To test this hypothesis, we chose muscovite ($KAl_2(Si_3Al)O_{10}(OH)_2$) as an example of minerals, and systematically studied the phase separation of poly (*L*-lysine) (PLL), quaternized dextran (Q-dextran), and single-stranded oligonucleotide (ss-oligo) on muscovite surface at varying mixing orders.

Muscovite is the most abundant rock-forming mineral on Earth and exists before the origin of life (Papineau, 2010; Hazen, 2013). It was proposed that life might originate in the space between mica flakes, especially muscovite mica (Hansma, 2009, 2010, 2013, 2014). Furthermore, muscovite mica is often used as a model mineral to study molecular adsorption, or a sample substrate for atomic force microscopy, surface force apparatus, and X-ray photoelectron spectroscopy (Binnig et al., 1986; Israelachvili and McGuiggan, 1988; Dufrêne, 2002; Wilson et al., 2002). It provides uniform and atomically flat surface when cleaved along the basal plane (De Poel et al., 2014). Such surface is a prerequisite for comparison of the coacervates under varying conditions. PLL, Q-dextran, and ss-oligo are examples of peptide, polysaccharides, and DNA, respectively. Results show that the coacervates with the most distinct morphologies and different dynamics are formed when Q-dextran firstly interacts with muscovite surface, indicating that polysaccharide was probably the first biopolymer synthesized and accumulated on the mineral surface in early Earth.

Materials and methods

Materials

21-mer single-stranded oligonucleotides of random sequence with and without Cy5 labeled on 5′-end were purchased from Invitrogen Biotechnology Co., Ltd. (Shanghai, China). Poly-*L*-lysine (PLL, M_W = 30–70 kDa) with and without fluorescein isothiocyanate (FITC) labeling were purchased from Sigma-Aldrich (St. Louis, MI). Dextran (M_W = 10 kDa) and tetramethylrhodamine labeled dextran (TRITC-dextran, M_W = 10 kDa) were purchased from Yuanye Biotechnology Co., Ltd. (Shanghai, China) and Sigma-Aldrich (St. Louis, MO), respectively. Quaternized dextran was synthesized in the lab by following a procedure described elsewhere (Mason et al., 2017). In brief, dextran was dissolved in NaOH solution, followed by the addition of 3-chloro-2-hydroxypropyltrimethylammonium chloride solution at 35°C. The mixture was left to react overnight. The ^{1}H NMR measurement on the final product revealed that each glucose carried 0.7 charge by average. Stock solutions of all samples were prepared in 20 mM MES buffer at pH 6.0 and diluted to known

concentrations before use. Muscovite mica was from Hebei, China.

Coacervation on muscovite surface

A lab-built sample cell was used to study the coacervation of PLL, ss-oligo, and Q-dextran. The freshly cleaved muscovite was glued between a cover glass (0.17 mm in thickness) and a glass chip of 5.0 mm in thickness. The glass chip was punctured with circular holes of 6.0 mm in diameter beforehand. The cover glass was the support of muscovite and also facilitated the observation by microscope.

The concentrations of PLL and Q-dextran were fixed at 1.0 mg/ml and 1.8 mg/ml, respectively. The concentrations of ss-oligo were 1.5, 3.0, and 6.0 mg/ml, corresponding to the +/− charge ratios (the number of amine groups over the number of phosphate groups, also named as N/P ratio) of 0.5, 1.0, and 2.0, after forming coacervates with PLL and Q-dextran at equal volume. The charges from the muscovite surface were not counted on the calculation of +/− ratios. Three different routes were applied to vary the mixing orders of PLL, ss-oligo, and ss-oligo.

Route 1: 20 μl Q-dextran was firstly applied on the muscovite surface. 5.0 min later, ss-oligo of same volume was added to formed complex or coacervate with Q-dextran. After incubated for 15 min, 20 μl PLL was added to initiate the formation of biphasic droplets on muscovite surface. The moment of adding PLL was set as time zero. This route was denoted as Q-dextran ← ss-oligo ← PLL.

Route 2: The mixing procedure and the incubation time in each step was the same as those in Route 1, except that the order of adding PLL and Q-dextran was reversed. Therefore, this route was denoted as PLL ← ss-oligo ← Q-dextran. The moment of adding Q-dextran in the last step was set as time zero.

Route 3: Equal volumes of PLL and Q-dextran were premixed in a centrifuge tube. 40 μl mixed solution was then applied to the muscovite surface. After 5 min, 20 μl ss-oligo was added to initiate the formation of biphasic droplet, and the moment of addition was set as time zero. This route was denoted as PLL/Q-dextran ← ss-oligo.

Confocal microscopy

The phase separation of Q-dextran, ss-oligo, and PLL on muscovite surface was monitored by laser scanning confocal microscope (LSCM, Nikon A1R-si). To enable observation by fluorescence, 1.0 wt% FITC-PLL, 1.0 wt% TRITC-Q-dextran, and 1.0 wt% Cy5-ss-oligo were premixed with the corresponding solutions beforehand. The excitation wavelengths for FITC, TRITC, and Cy5 were 490 nm, 557 nm, and 649 nm, respectively. All the settings on LSCM were kept constant during the experiments. The visualization and analysis of the fluorescence images were conducted by using ImageJ software. The average fluorescence intensity at selected time points was calculated to quantitatively describe the growth or dissociation rate of the phases. The fluorescence intensity was normalized by the highest value to compare the behaviors of different phases in one plot. The area occupied by the phases normalized by the total area was also calculated in certain cases.

Results and discussion

There are four different types of polyelectrolytes in the system if treating muscovite surface as a 2D and rigid polyanion. The charge density of PLL (4.8 mmol/g, as calculated by the number of charges per molecular weight of monomer) is almost doubled that of Q-dextran (2.7 mmol/g), and its backbone is also more hydrophobic. Therefore, PLL has the priority to form complex with ss-oligo or attach on the muscovite surface under the same conditions. Similarly, the muscovite surface contains 2.1×10^{14} charges per square cm (Güven, 1971), far less than that of ss-oligo. It is inferior to ss-oligo in forming complex with polycations. The total negative charges on the muscovite bottom area of 6.0 mm in diameter is 5.9×10^{13}, which is several orders lower than that provided by 20 μl ss-oligo at 1.5 mg/ml. Therefore, the muscovite surface generates negligible effect on the +/− charge ratio. To enhance the effect of muscovite surface on the phase separation process, and also to better mimic the prebiotic condition under which the biopolymers may interact with the mineral surface in sequence, we designed three Routes (Q-dextran ← ss-oligo ← PLL, PLL ← ss-oligo ← Q-dextran, and PLL/Q-dextran ← ss-oligo), allowing Q-dextran, PLL, and their mixture to firstly contact with the muscovite surface, separately, for 5 min, followed by the addition of ss-oligo. In each route, all the conditions are kept constant except that the ss-oligo concentration is varied, to tune the +/− charge ratio from 0.5 to 2.0.

Route 1: Q-dextran ← ss-oligo ← PLL

In this route, 1.8 mg/ml Q-dextran was firstly applied to the muscovite surface for 5 min. Since the diffusion coefficient and the charge density of Q-dextran with M_w = 10 kDa are known (Venturoli and Rippe, 2005; Goins et al., 2008), calculation shows that about half of the negative charges on muscovite surface are neutralized. Ss-oligo at different concentrations is then added to form complex with Q-dextran in the solution and on the surface. Images are taken after incubation for 15 min. With decreasing ss-oligo concentration from 6.0 to 1.5 mg/ml, the coacervation of Q-dextran and ss-oligo on the muscovite surface becomes stronger as demonstrated by the fluorescence intensity and the

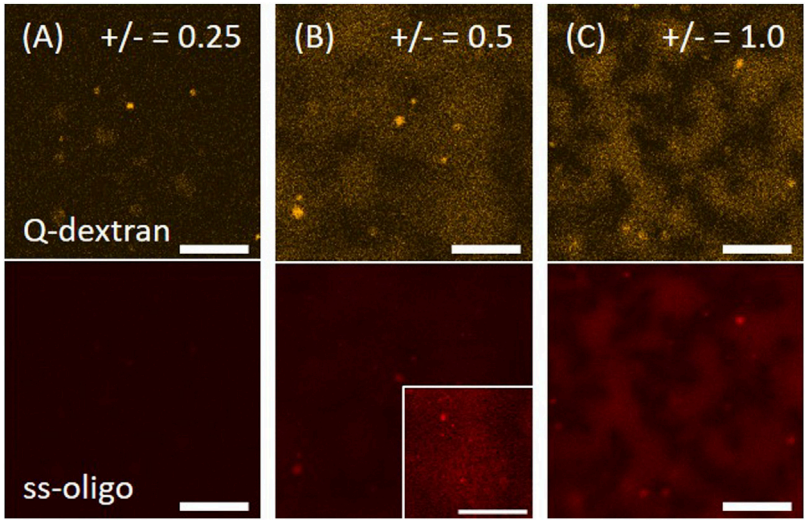

FIGURE 1
Coacervation of Q-dextran and ss-oligo on muscovite surface. The concentrations of ss-oligo were **(A)** 6.0 mg/ml, **(B)** 3.0 mg/ml, and **(C)** 1.5 mg/ml. Q-dextran at 1.8 mg/ml was applied 5.0 min earlier than ss-oligo. The orange and red color denote the traces of TRITC-Q-dextran and Cy5-ss-oligo, respectively. The contract of the right corner in **(B)** is enhanced to show the distribution of ss-oligo. Scale bars, 20 μm.

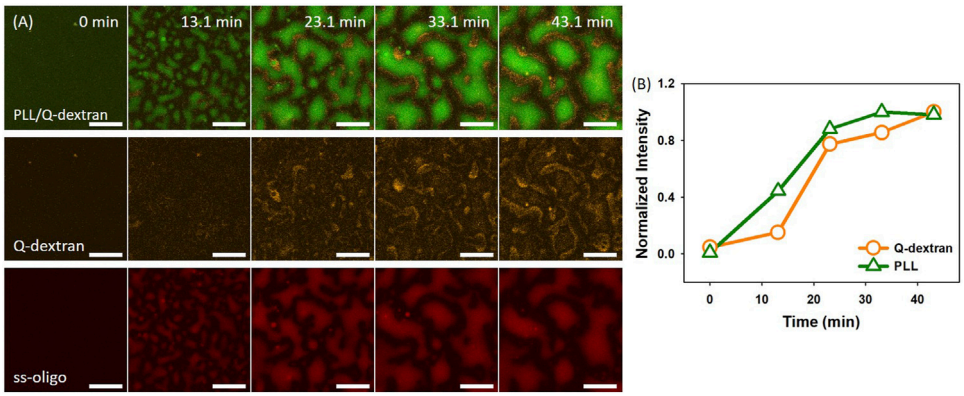

FIGURE 2
Coacervation on muscovite surface *via* Q-dextran ← ss-oligo ← PLL. The concentrations of ss-oligo, Q-dextran and PLL are 6.0, 1.8, and 1.0 mg/ml, respectively. The final +/− ratio is 0.5. **(A)** Time series of images showing the phase separation by overlay of FITC-PLL/TRITC-Q-dextran (green and orange), TRITC-Q-dextran (orange), and Cy5-ss-oligo phase (red), scale bars: 20 μm. **(B)** Time dependence of the normalized intensity of PLL and Q-dextran.

size of the coacervates (Figure 1). It is reasonable as the +/− charge ratio of the Q-dextran/ss-oligo coacervates increases from 0.25 to unity. The neutralization of the charges results in the formation of coacervates with larger size and higher chain density (Luo and Wang, 2014).

1.0 mg/ml PLL was applied to initiate the formation of biphasic droplets. The process is highly dependent on the ss-oligo concentration or the overall +/− charge ratio. In the case of 6.0 mg/mL ss-oligo, the +/− ratio increases from 0.25 to 0.50 after the addition of PLL. The interaction of PLL with the extra ss-oligo molecules results in a heavy coacervation of both PLL/ss-oligo phase and Q-dextran/ss-oligo phase, as demonstrated by the fast growth of the two phases (Figure 2A, 2B, and Movie S1, S2). Note that each phase contains all the three components. For simplicity, only the two major components are mentioned to distinguish the phases. Fluorescence intensity indicates that concentration of ss-oligo is much higher in PLL-rich phase (Figure 2A).

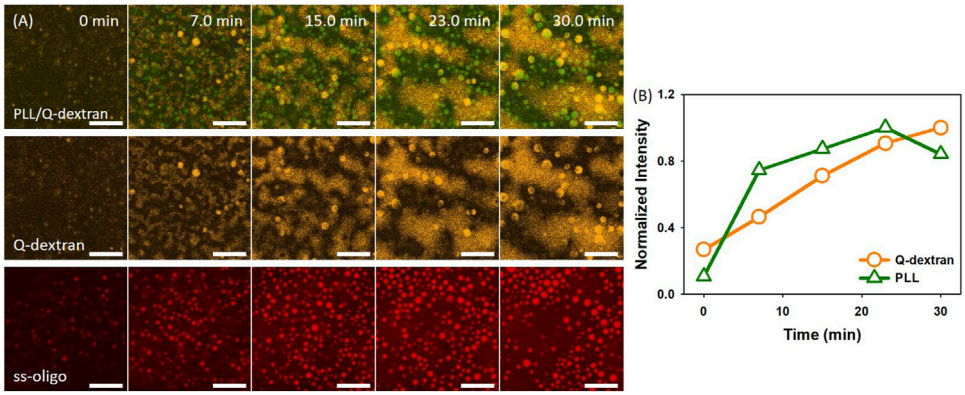

FIGURE 3
Coacervation on muscovite surface *via* Q-dextran ← ss-oligo ← PLL. The concentrations of ss-oligo, Q-dextran and PLL are 3.0, 1.8, and 1.0 mg/ml, respectively. The final +/− ratio is 1.0. **(A)** Time series of images showing the phase separation by overlay of FITC-PLL/TRIRC-Q-dextran (green and orange), TRIRC-Q-dextran (orange), and Cy5-ss-oligo phase (red). Scale bars: 20 μm. **(B)** Time dependence of the normalized intensity of PLL and Q-dextran.

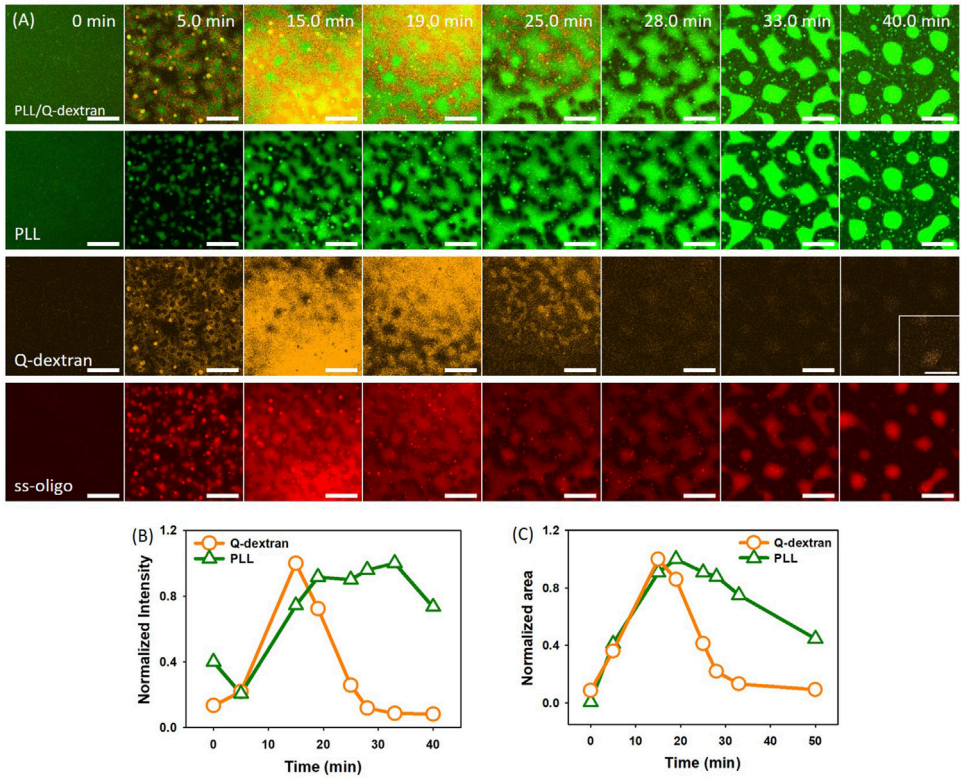

FIGURE 4
Coacervation on muscovite surface *via* Q-dextran ← ss-oligo ← PLL. The concentrations of ss-oligo, Q-dextran and PLL are 1.5, 1.8, and 1.0 mg/ml, respectively. The final +/− ratio is 2.0. **(A)** Time series of images showing the phase separation by FITC-PLL/(green), TRITC-Q-dextran (orange), Cy5-ss-oligo phase (red), and overlay of PLL and Q-dextran. Scale bars: 20 μm. **(B)** Time dependence of the normalized intensity of PLL and Q-dextran. **(C)** Time dependence of the normalized area of PLL and Q-dextran.

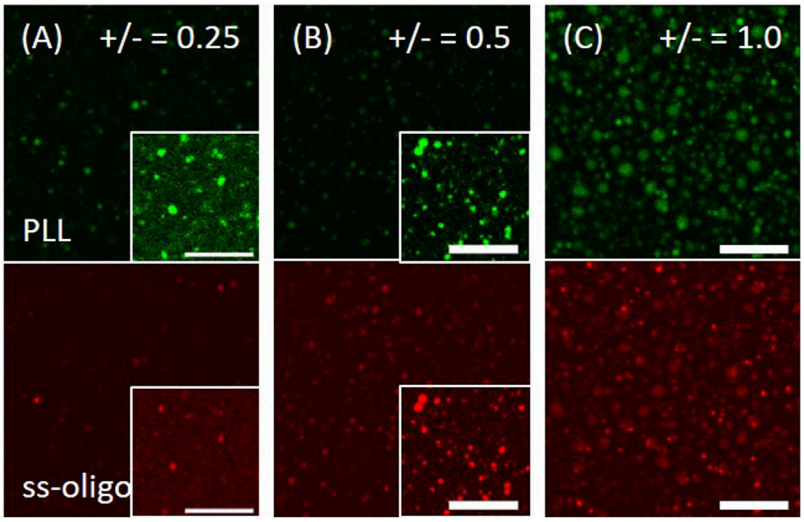

FIGURE 5
Coacervation of PLL and ss-oligo on muscovite surface. The concentrations of ss-oligo were **(A)** 6.0 mg/ml, **(B)** 3.0 mg/ml, and **(C)** 1.5 mg/ml. The right corner in the selected panels shows the same image but intensified 10 times to reveal the phases. PLL at 1.0 mg/ml was applied 5.0 min earlier than ss-oligo. The green and red color denote the traces of FITC-PLL and Cy5-ss-oligo, respectively. Scale bars, 20 μm.

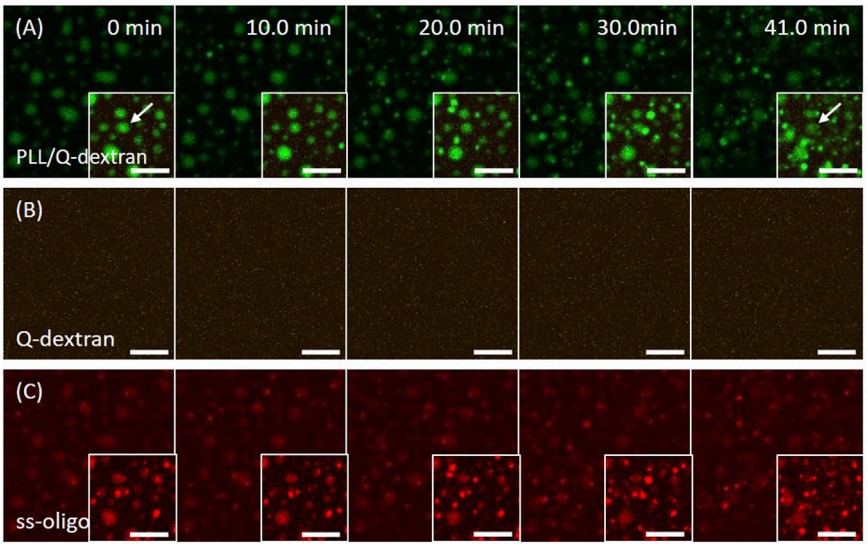

FIGURE 6
Coacervation on muscovite surface *via* PLL ← ss-oligo ←Q-dextran. The concentrations of ss-oligo, Q-dextran and PLL are 1.5, 1.8, and 1.0 mg/ml, respectively. The final +/− ratio is 2.0. **(A)** Time series of images showing the phase separation by **(A)** overlay of FITC-PLL/TRITC-Q-dextran (green/orange), **(B)** TRITC-Q-dextran (orange), and **(C)** Cy5-ss-oligo phase (red). Scale bars: 10 μm.

Because Q-dextran is coated on the muscovite surface beforehand, the Q-dextran/ss-oligo phase is continuous, while the PLL/ss-oligo phase is isolated. Another interesting feature is that the continuous Q-dextran/ss-oligo phase is not uniform in component distribution, but forms wrinkles around the PLL/ss-oligo phases especially at the later stage (Movie S2). We attribute it to the elevated ss-oligo concentration in PLL/ss-oligo phase, which generates a strong coacervation of Q-dextran and ss-oligo in the periphery of the PLL/ss-oligo phase.

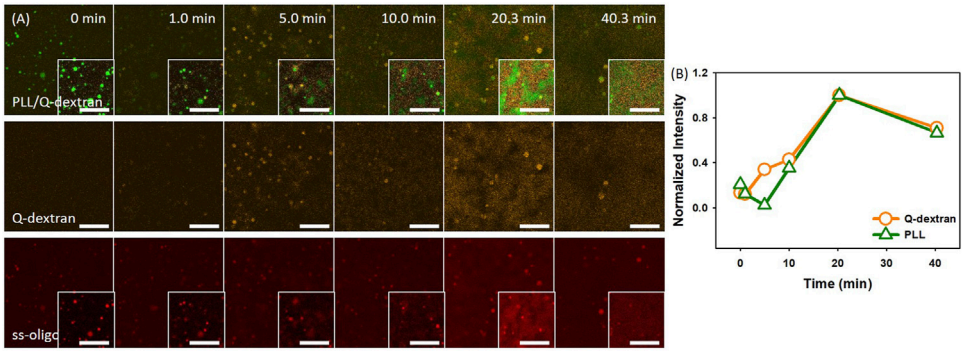

FIGURE 7
Coacervation on muscovite surface *via* PLL ← ss-oligo ←Q-dextran. The concentrations of ss-oligo, Q-dextran and PLL are 3.0, 1.8, and 1.0 mg/ml, respectively. The final +/− ratio is 1.0. **(A)** Time series of images showing the phase separation by overlay of FITC-PLL/TRITC-Q-dextran (green/orange), TRITC-Q-dextran (orange), and Cy5-ss-oligo phase (red). Scale bars: 20 μm. **(B)** Time dependence of the normalized intensity of PLL and Q-dextran.

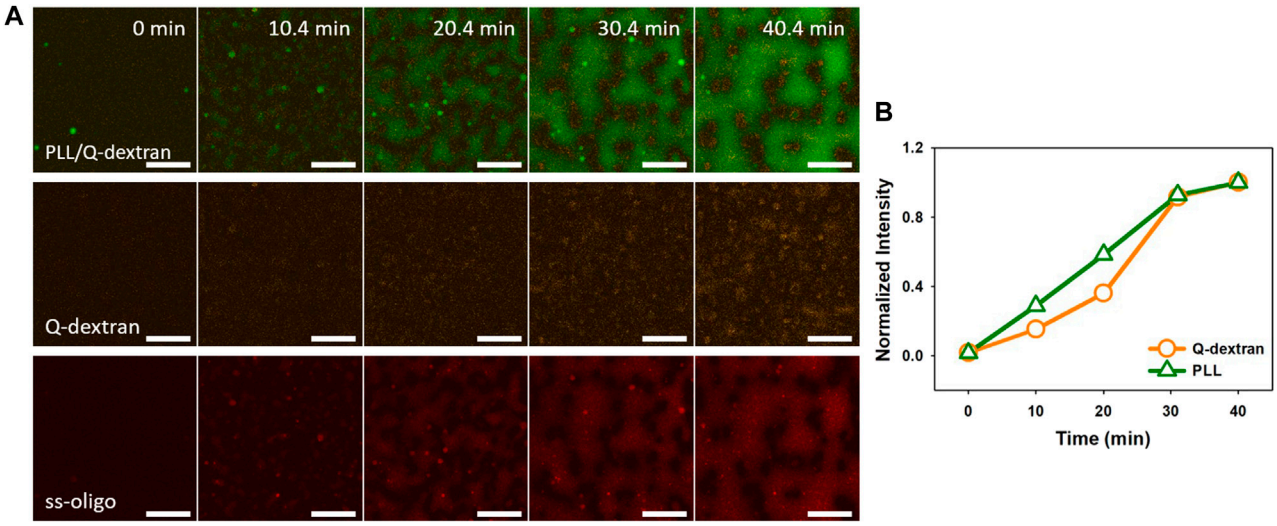

FIGURE 8
Coacervation on muscovite surface *via* PLL ← ss-oligo ←Q-dextran. The concentrations of ss-oligo, Q-dextran and PLL are 6.0, 1.8, and 1.0 mg/ml, respectively. The final +/− ratio is 0.5. Time series of images showing the phase separation by overlay of FITC-PLL/TRITC-Q-dextran (green/orange), TRITC-Q-dextran (orange), and Cy5-ss-oligo phase (red). Scale bars: 20 μm.

In the case of 3.0 mg/ml ss-oligo, the addition of PLL increases the +/− ratio from 0.50 to 1.0, indicating that the excess ss-oligo molecules form complex with PLL at unified +/− ratio. Spherical PLL/ss-oligo coacervates are formed and float in the solution instead attaching on the surface (Movie S3). Both the size and the number of such coacervates increase with time. The spherical shape is maintained throughout the studied time period (Figure 3A). The Q-dextran/ss-oligo phase exhibits quite different behavior. A fast growth and spreading on the muscovite surface occur with time (Figure 3A, 3B and Movie S4). Some spherical droplets are also shown in Q-dextran channel, especially in the later stage, but these are the same droplets observed in PLL channel. It is normal to form spherical droplets containing both PLL and Q-dextran at elevated concentrations at +/- = 1.0. Again, ss-oligo molecules mainly stay with PLL (Figure 3A).

In the case of 1.5 mg/ml ss-oligo, all ss-oligo molecules form coacervates with Q-dextran. The addition of PLL increases the +/− ratio from 1.0 to 2.0, and polycations are in excess. A fast growth of both PLL/ss-oligo phase and Q-dextran/oligo phase on the muscovite surface occurs at early stage. As the content of PLL reaches a certain value, the Q-dextran/ss-oligo phase is not stable. It undergoes a swelling and dissociation process to detach from the muscovite surface, followed by escaping of the majority

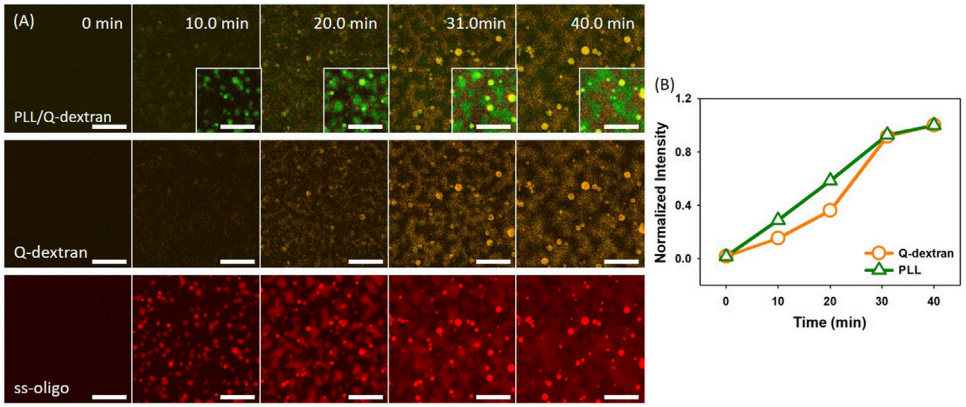

FIGURE 9
Coacervation on muscovite surface *via* PLL/ss-oligo ←Q-dextran. The concentrations of ss-oligo, Q-dextran and PLL are 1.5, 1.8, and 1.0 mg/ml, respectively. The final +/− ratio is 2.0. **(A)** Time series of images showing the phase separation by overlay of FITC-PLL/TRITC-Q-dextran (green/orange), TRITC-Q-dextran (orange), and Cy5-ss-oligo phase (red). Scale bars: 20 μm. **(B)** Time dependence of the normalized intensity of PLL and Q-dextran.

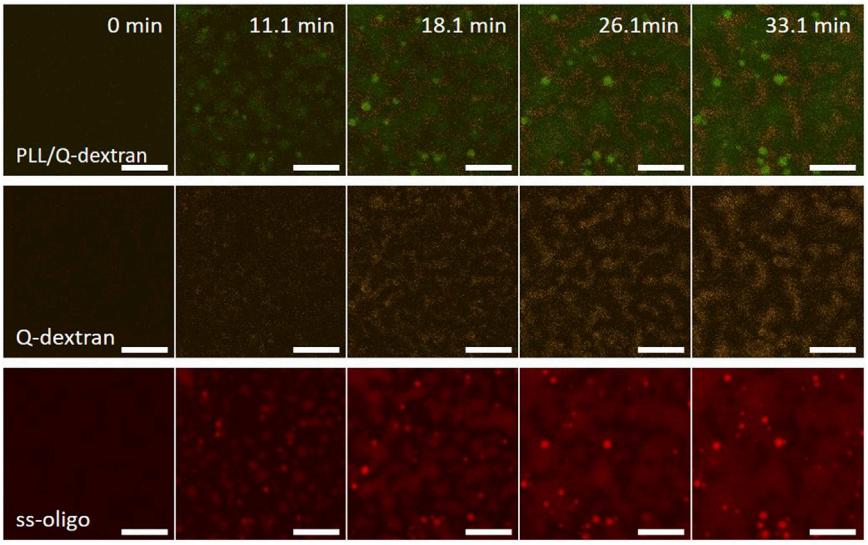

FIGURE 10
Coacervation on muscovite surface *via* PLL/ss-oligo ← Q-dextran. The concentrations of ss-oligo, Q-dextran and PLL are 3.0, 1.8, and 1.0 mg/ml, respectively. The final +/− ratio is 1.0. Time series of images showing the phase separation by overlay of FITC-PLL/TRITC-Q-dextran (green/orange), TRITC-Q-dextran (orange), and Cy5-ss-oligo phase (red). Scale bars: 20 μm.

of Q-dextran and less amount of ss-oligo (Figure 4A, 4B and Movie S5, S6). The PLL/ss-oligo phase still grows but at a much lower rate during the release of Q-dextran/ss-oligo phase. As more ss-oligo molecules are captured, the PLL/ss-oligo phase shrink into spherical shape (Figure 4C and Movie S6, S7). The amount of Q-dextran reaches minimum and mainly stays as the minor component of the PLL/ss-oligo phase.

Route 2: PLL ← ss-oligo ← Q-dextran

PLL at 1.0 mg/ml is firstly applied on muscovite surface, followed by the addition of ss-oligo 5.0 min later. PLL and ss-oligo form spherical coacervate on the mineral surface at all the studied +/− ratios, with the heaviest coacervation occurring at +/− = 1.0 (Figure 5). Different from the behavior of Q-dextran/ss-oligo (Figure 1), the PLL/ss-oligo coacervate does not form an

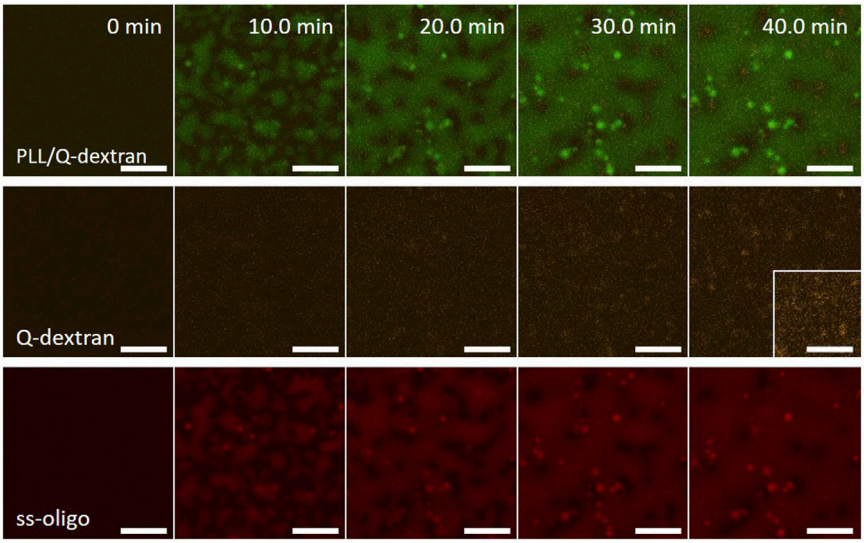

FIGURE 11
Coacervation on muscovite surface *via* PLL/ss-oligo ← Q-dextran. The concentrations of ss-oligo, Q-dextran and PLL are 6.0, 1.8, and 1.0 mg/ml, respectively. The final +/− ratio is 0.5. Time series of images showing the phase separation by overlay of FITC-PLL/TRITC-Q-dextran (green/orange), TRITC-Q-dextran (orange), and Cy5-ss-oligo phase (red). Scale bars: 20 μm.

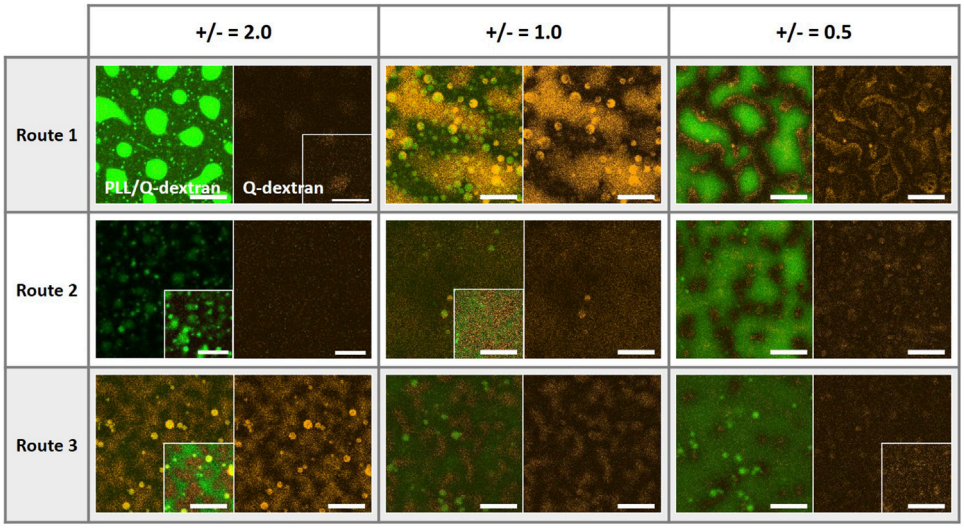

FIGURE 12
Coacervates on the muscovite surfaces at the ending stage as formed by different mixing orders and at +/− ratios of 0.5, 1.0, and 2.0. The green, red, and orange color denote the traces of PLL, ss-oligo and Q-dextran, respectively. Scale bars, 20 μm.

effective coating. We attribute it to the hydrophobicity of PLL/ss-oligo, which reduces its wetting ability on the hydrophilic muscovite surface.

The addition of Q-dextran 15 min later initiates the formation of biphasic coacervates. The process is dependent on the concentration of ss-oligo or +/− charge ratio. In the case of 1.5 mg/ml ss-oligo, all ss-oligo molecules basically form coacervates with PLL in the first place. Because ss-oligo has the priority to form complex with PLL, the addition of Q-dextran does not generate prominent effect on the coacervation on

muscovite surface as indicated by the fluorescence intensity (Figure 6B). However, the deviation of +/− ratio from unity to 2.0 results in a slow dissociation of larger size PLL/ss-oligo coacervates (indicated by the arrow in Figure 6A), together with the formation of spherical droplets floating in the solution (Figure 6A and 6B, Movie S8).

In the case of 3.0 mg/ml ss-oligo, the addition of Q-dextran increases the +/− ratio from 0.50 to 1.0, indicating that all the ss-oligo molecules form complex with PLL or Q-dextran. A fast growth of both PLL/ss-oligo and Q-dextran/ss-oligo occurs with time (Figure 7A and 7B). The Q-dextran/ss-oligo phase has the tendency to spread all over the muscovite surface (Movie S9), while the PLL/ss-oligo phase forms cluster structure *via* growth and fusion on the top of the continuous Q-dextran/ss-oligo phase (Movie S10). The decrease of the fluorescence intensity for all the three components in the ending stage (40.3 min) is probably caused by the mingling of the two phases.

In the case of 6.0 mg/mL ss-oligo, the amount of ss-oligo is in excess before and after the addition of Q-dextran, indicating that all PLL and Q-dextran form complex or coacervates with ss-oligo. Similar as the phase separation in 3.0 mg/mL ss-oligo (Figure 7), the Q-dextran/ss-oligo phase spreads on the muscovite surface, while the PLL/ss-oligo phase forms clusters and then network on the top of the continuous Q-dextran/ss-oligo phase (Figure 8, Movie S11, S12). The borderline between the two phase are more distinct than that in 3.0 mg/mL ss-oligo.

Route 3: PLL/Q-dextran ← ss-oligo

The above results indicate that PLL and ss-oligo form stable coacervates under all the studied conditions, as demonstrated by their coincident fluorescence intensity, while Q-dextran/ss-oligo phase exhibits stronger capacity to coat the muscovite surface. The strong coating ability is attributed to the hydrogen bonding between Q-dextran and the muscovite surface (Jucker et al., 1997; Kwon et al., 2006). As the mixture of PLL and Q-dextran is firstly applied on the muscovite surface, followed by the addition of ss-oligo 5 min later, the phase separation process is determined by property of both PLL and Q-dextran.

In the case of 1.5 mg/ml ss-oligo, the charge ratio is 2.0, and polycations are in excess. Because Q-dextran is coated on the muscovite surface beforehand and concentrated, ss-oligo has the tendency to form coacervate with the Q-dextran coating (Figure 9, Movie S13). Besides being the minor component of the Q-dextran/ss-oligo phase (Figure 9B, Movie S14), PLL and ss-oligo mainly form spherical droplets which float in the solution.

In the case of 3.0 mg/ml ss-oligo, the ± charge ratio is unity. Similar situation is observed. Heavy coacervation of Q-dextran and ss-oligo occurs on the muscovite surface because of the coating beforehand (Figure 10). Meantime, PLL and ss-oligo form spherical droplets and stay mainly in the solution. In the later stage, however, a few PLL/ss-oligo droplets attach on the coated Q-dextran/ss-oligo phase (Figure 10 and Movie S15).

In the case of 6.0 mg/ml ss-oligo, the +/− charge ratio is 0.5. All PLL and Q-dextran form coacervate with ss-oligo. The excess ss-oligo renders the Q-dextran/ss-oligo complex negative in nature, leading to weak Q-dextran/ss-oligo coating on the muscovite surface (Figure 11). PLL and ss-oligo mainly form spherical droplets in the early stage. Driven by gravity, the PLL/ss-oligo droplets fall on the muscovite surface and fuse into a "blanket", covering most of the surface (Figure 11).

Conclusion

The coacervates of PLL, ss-oligo, and Q-dextran exhibit different morphologies on the muscovite surface, which is highly dependent on the mixing order and the +/− ratios. It is the interplay of the four charged components (muscovite surface is treated as a polyanion) that determines the kinetics and the structure of the coacervates. Clearly, the charge density and hydrophobicity play key roles during the coacervation process. A comparison of the size and intensity of the coacervates (Figure 12) indicates that the Route 1, in which Q-dextran firstly interacts with the muscovite surface, generates the most distinct and versatile morphologies, including the spherical PLL/ss-oligo droplets on the surface at +/− = 2.0, floating PLL/ss-oligo droplets above the Q-dextran/ss-oligo blanket on the surface at +/− - = 1.0, and PLL/ss-oligo islands surrounded by the Q-dextran/ss-oligo sea at +/− = 0.5. Moreover, the kinetic path of each morphology is specific as indicated the supplementary movies. For example, the PLL-ss-oligo droplets on the surface is formed by forced dissociation of Q-dextran/ss-oligo phase, with Q-dextran being expelled and ss-oligo being captured (Figure 4 and Supplementary Movies S5~S7). In Route two and Route 3, the coacervations on the muscovite surface are much weaker in most of the cases as indicated the fluorescence intensity. The coacervates at different charge ratios are also formed by similar path way: the intensity of both PLL and Q-dextran monotonously increase with time.

Formation of protocell with hierarchical structures and desirable biofunctions is the bridge from non-living matter to life. The morphologies (Figure 12) and the formation pathways of the coacervates on muscovite surface suggest that polysaccharide is probably the first biopolymer synthesized and accumulated on the mineral surface, which provides a "nest" for protein/peptide and DNA/RNA to from sub-compartments and to further develop advanced functions. Different from peptide and DNA, polysaccharides possess hydrophilic backbone and cannot be hydrolyzed in aqueous solution at normal conditions. On one hand, polysaccharides can reach much higher concentration in water. On the other hand, polysaccharides can retain large amount of water in the presence of hydrophobic biopolymers, such as peptides and lipids. More importantly, polysaccharides

can wet the mineral surface in most of the cases, serving as a lubricate or protecting layer to ensure the integrity and mobility of other biopolymers. Taken together, our work provides a further understanding of the functions of biopolymers and their evolution pathway into protocell and possibly first life in the early Earth.

Data availability statement

The original contributions presented in the study are included in the article/supplementary material, further inquiries can be directed to the corresponding author

Author contributions

JC, YL, YL, and DL designed experiments. JC performed the experiments and analysed the results. ZL and QB assisted in analysing the results. JC and DL wrote the manuscript. All authors contributed to the article and approved the final manuscript.

Funding

Financial support of this work from the National Natural Science Foundation of China (21973002) is gratefully acknowledged. The measurements of LCSM were performed at the Analytical Instrumentation Center of Peking University. We acknowledge the assistance and support from PKUAIC (Yan Guan).

Conflict of interest

The authors declare that the research was conducted in the absence of any commercial or financial relationships that could be construed as a potential conflict of interest.

Publisher's note

All claims expressed in this article are solely those of the authors and do not necessarily represent those of their affiliated organizations, or those of the publisher, the editors and the reviewers. Any product that may be evaluated in this article, or claim that may be made by its manufacturer, is not guaranteed or endorsed by the publisher.

Supplementary Material

The Supplementary Material for this article can be found online at: https://www.frontiersin.org/articles/10.3389/frsfm.2022.1054658/full#supplementary-material

References

Abbas, M., Lipiński, W. P., Wang, J., and Spruijt, E. (2021). Peptide-based coacervates as biomimetic protocells. *Chem. Soc. Rev.* 50, 3690–3705. doi:10.1039/D0CS00307G

Alberti, S., Gladfelter, A., and Mittag, T. (2019). Considerations and challenges in studying liquid-liquid phase separation and biomolecular condensates. *Cell* 176, 419–434. doi:10.1016/j.cell.2018.12.035

Bernal, J. D. (1951). *The physical basis of life*. London, UK: Routledge and Kegan Paul.

Binnig, G., Quate, C. F., and Gerber, C. (1986). Atomic force microscope. *Phys. Rev. Lett.* 56 (9), 930–933. doi:10.1103/PhysRevLett.56.930

Black, K. A., Priftis, D., Perry, S. L., Yip, J., Byun, W. Y., and Tirrell, M. (2014). Protein encapsulation via polypeptide complex coacervation. *ACS Macro Lett.* 3, 1088–1091. doi:10.1021/mz500529v

Brangwynne, C. P., Eckmann, C. R., Courson, D. S., Rybarska, A., Hoege, C., Gharakhani, J., et al. (2009). Germline P granules are liquid droplets that localize by controlled dissolution/condensation. *Science* 324, 1729–1732. doi:10.1126/science.1172046

Brangwynne, C. P. (2013). Phase transitions and size scaling of membrane-less organelles. *J.Cell Biol.* 203, 875–881. doi:10.1083/jcb.201308087

Chen, Y., Yuan, M., Zhang, Y., Liu, S., Yang, X., Wang, K., et al. (2020). Construction of coacervate-in-coacervate multi-compartment protocells for spatial organization of enzymatic reactions. *Chem. Sci.* 11, 8617–8625. doi:10.1039/d0sc03849k

Croguennec, T., Tavares, G. M., and Bouhallab, S. (2017). Heteroprotein complex coacervation: A generic process. *Adv. Colloid Interface Sci.* 239, 115–126. doi:10.1016/j.cis.2016.06.009

Dalai, P., Kaddour, H., and Sahai, N. (2016). Incubating life: Prebiotic sources of organics for the origin of life. *Elements* 12, 401–406. doi:10.2113/gselements.12.6.401

Dalai, P., and Sahai, N. (2019). Mineral–lipid interactions in the origins of life. *Trends biochem. Sci.* 44, 331–341. doi:10.1016/j.tibs.2018.11.009

De Poel, W., Pintea, S., Drnec, J., Carla, F., Felici, R., Mulder, P., et al. (2014). Muscovite mica: Flatter than a pancake. *Surf. Sci.* 619, 19–24. doi:10.1016/j.susc.2013.10.008

Douliez, J. P., Martin, N., Gaillard, C., Beneyton, T., Baret, J. C., Mann, S., et al. (2017). Catanionic coacervate droplets as a surfactant-based membrane-free protocell model. *Angew. Chem.* 129, 13877–13881. doi:10.1002/ange.201707139

Dufrêne, Y. F. (2002). Atomic force microscopy, a powerful tool in microbiology. *J. Bacteriol.* 184 (19), 5205–5213. doi:10.1128/JB.184.19.5205-5213.2002

Dzieciol, A. J., and Mann, S. (2012). Designs for life: Protocell models in the laboratory. *Chem. Soc. Rev.* 41, 79–85. doi:10.1039/C1CS15211D

Ertem, G., and Ferris, J. P. (1996). Synthesis of RNA oligomers on heterogeneous templates. *Nature* 379, 238–240. doi:10.1038/379238a0

Ertem, G. (2021). The role of minerals in events that led to the origin of life. *Astrobiology* 21, 137–150. doi:10.1089/ast.2020.2245

Feric, M., Vaidya, N., Harmon, T. S., Mitrea, D. M., Zhu, L., Richardson, T. M., et al. (2016). Coexisting liquid phases underlie nucleolar subcompartments. *Cell* 165, 1686–1697. doi:10.1016/j.cell.2016.04.047

Ferris, J. P., Hill, A. R., Liu, R., and Orgel, L. E. (1996). Synthesis of long prebiotic oligomers on mineral surfaces. *Nature* 381, 59–61. doi:10.1038/381059a0

Ferris, J. P. (2002). Montmorillonite catalysis of 30–50 mer oligonucleotides: Laboratory demonstration of potential steps in the origin of the RNA world. *Orig. Life Evol. Biosph.* 32, 311–332. doi:10.1023/A:1020543312109

Franchi, M., and Gallori, E. (2005). A surface-mediated origin of the RNA world: Biogenic activities of clay-adsorbed RNA molecules. *Gene* 346, 205–214. doi:10.1016/j.gene.2004.11.002

Gan, H., Tang, K., Sun, T., Hirtz, M., Li, Y., Chi, L., et al. (2009). Selective adsorption of DNA on chiral surfaces: Supercoiled or relaxed conformation. *Angew. Chem. Int. Ed.* 48, 5282–5286. doi:10.1002/anie.200806295

Ghosh, B., Bose, R., and Tang, T. Y. D. (2021). Can coacervation unify disparate hypotheses in the origin of cellular life? *Curr. Opin. Colloid Interface Sci.* 52, 101415. doi:10.1016/j.cocis.2020.101415

Goins, A. B., Sanabria, H., and Waxham, M. N. (2008). Macromolecular crowding and size effects on probe microviscosity. *Biophys. J.* 95, 5362–5373. doi:10.1529/biophysj.108.131250

Gomes, E., and Shorter, J. (2019). The molecular language of membraneless organelles. *J. Biol. Chem.* 294, 7115–7127. doi:10.1074/jbc.tm118.001192

Gomez, F., Aguilera, A., and Amils, R. (2007). Soluble ferric iron as an effective protective agent against UV radiation: Implications for early life. *Icarus* 191, 352–359. doi:10.1016/j.icarus.2007.04.008

Güven, N. (1971). The crystal structures of 2 M_1 phengite and 2 M_1 muscovite. *Z. fur Kristallogr. - Cryst. Mater.* 134, 196–212. doi:10.1524/zkri.1971.134.16.196

Hanczyc, M. M., Mansy, S. S., and Szostak, J. W. (2007). Mineral surface directed membrane assembly. *Orig. Life Evol. Biosph.* 37, 67–82. doi:10.1007/s11084-006-9018-5

Hansma, H. G. (2009). Could life originate between mica sheets?: Mechanochemical biomolecular synthesis and the origins of life. *MRS Proc.* 1185 (1), 20–25. doi:10.1557/PROC-1185-II03-15

Hansma, H. G. (2010). Possible origin of life between mica sheets. *J. Theor. Biol.* 266 (1), 175–188. doi:10.1016/j.jtbi.2010.06.016

Hansma, H. G. (2013). Possible origin of life between mica sheets: Does life imitate mica? *J. Biomol. Struct. Dyn.* 31 (8), 888–895. doi:10.1080/07391102.2012.718528

Hansma, H. G. (2014). The power of crowding for the origins of life. *Orig. Life Evol. Biosph.* 44 (4), 307–311. doi:10.1007/s11084-014-9382-5

Hazen, R. M., Filley, T. R., and Goodfriend, G. A. (2001). Selective adsorption of *L*- and *D*-amino acids on calcite: Implications for biochemical homochirality. *Proc. Natl. Acad. Sci. U. S. A.* 98, 5487–5490. doi:10.1073/pnas.101085998

Hazen, R. M. (2013). Paleomineralogy of the hadean eon: A preliminary species list. *Am. J. Sci.* 313, 807–843. doi:10.2475/09.2013.01

Huang, W., and Ferris, J. P. (2003). Synthesis of 35–40 mers of RNA oligomers from unblocked monomers. A simple approach to the RNA world. *Chem. Commun.* 21, 1458–1459. doi:10.1039/B303134A

Hyman, A. A., Weber, C. A., and Julicher, F. (2014). Liquid-liquid phase separation in biology. *Annu. Rev. Cell Dev. Biol.* 30, 39–58. doi:10.1146/annurev-cellbio-100913-013325

Israelachvili, J. N., and McGuiggan, P. M. (1988). Forces between surfaces in liquids. *Science* 241 (4867), 795–800. doi:10.1126/science.241.4867.795

Jiang, L., Shao, C., Wu, Q.-J., Chen, G., Zhou, J., Yang, B., et al. (2017). NEAT1 scaffolds RNA-binding proteins and the microprocessor to globally enhance pri-miRNA processing. *Nat. Struct. Mol. Biol.* 24, 816–824. doi:10.1038/nsmb.3455

Jonsson, C. M., Jonsson, C. L., Sverjensky, D. A., Cleaves, H. J., and Hazen, R. M. (2009). Attachment of *L*-glutamate to rutile (α-TiO_2): A potentiometric, adsorption, and surface complexation study. *Langmuir* 25, 12127–12135. doi:10.1021/la901635t

Jucker, B., Harms, H., Hug, S., and Zehnder, A. (1997). Adsorption of bacterial surface polysaccharides on mineral oxides is mediated by hydrogen bonds. *Colloids Surfaces B Biointerfaces* 9, 331–343. doi:10.1016/s0927-7765(97)00038-6

Kawamura, K., Takeya, H., Kushibe, T., and Koizumi, Y. (2011). Mineral-enhanced hydrothermal oligopeptide formation at the second time scale. *Astrobiology* 11, 461–469. doi:10.1089/ast.2011.0620

Kee, T. P., and Monnard, P.-A. (2016). On the emergence of a proto-metabolism and the assembly of early protocells. *Elements* 12, 419–424. doi:10.2113/gselements.12.6.419

Koga, S., Williams, D. S., Perriman, A. W., and Mann, S. (2011). Peptide–nucleotide microdroplets as a step towards a membrane-free protocell model. *Nat. Chem.* 3, 720–724. doi:10.1038/nchem.1110

Kruif, C., Weinbreck, F., and Vries, R. D. (2005). Complex coacervation of proteins and anionic polysaccharides. *Curr. Opin. Colloid Interface Sci.* 9, 340–349.

Kumar, B. P., Fothergill, J., Bretherton, J., Tian, L., Patil, A. J., Davis, S. A., et al. (2018). Chloroplast-containing coacervate micro-droplets as a step towards photosynthetically active membrane-free protocells. *Chem. Commun.* 54, 3594–3597. doi:10.1039/c8cc01129j

Kwon, K. D., Green, H., Bjöörn, P., and Kubicki, J. D. (2006). Model bacterial extracellular polysaccharide adsorption onto silica and alumina: Quartz crystal microbalance with dissipation monitoring of dextran adsorption. *Environ. Sci. Technol.* 40, 7739–7744. doi:10.1021/es061715q

Lahav, N., and Chang, S. (1976). The possible role of solid surface area in condensation reactions during chemical evolution: Reevaluation. *J. Mol. Evol.* 8, 357–380. doi:10.1007/bf01739261

Li, H., Zhang, F., Zhang, Y., Ye, M., Zhou, B., Tang, Y.-Z., et al. (2009). Peptide diffusion and self-assembly in ambient water nanofilm on mica surface. *J. Phys. Chem. B* 113, 8795–8799. doi:10.1021/jp903446g

Liao, H.-S., Lin, J., Liu, Y., Huang, P., Jin, A., and Chen, X. (2016). Self-assembly mechanisms of nanofibers from peptide amphiphiles in solution and on substrate surfaces. *Nanoscale* 8, 14814–14820. doi:10.1039/c6nr04672j

Luo, Y., and Wang, Q. (2014). Recent development of chitosan-based polyelectrolyte complexes with natural polysaccharides for drug delivery. *Int. J. Biol. Macromol.* 64, 353–367. doi:10.1016/j.ijbiomac.2013.12.017

Martin, N., Li, M., and Mann, S. (2016). Selective uptake and refolding of globular proteins in coacervate microdroplets. *Langmuir* 32, 5881–5889. doi:10.1021/acs.langmuir.6b01271

Martra, G., Deiana, C., Sakhno, Y., Barberis, I., Fabbiani, M., Pazzi, M., et al. (2014). The formation and self-assembly of long prebiotic oligomers produced by the condensation of unactivated amino acids on oxide surfaces. *Angew. Chem. Int. Ed. Engl.* 53, 4759–4762. doi:10.1002/ange.201311089

Mason, A. F., Buddingh', B. C., Williams, D. S., and van Hest, J. C. M. (2017). Hierarchical self-assembly of a copolymer-stabilized coacervate protocell. *J. Am. Chem. Soc.* 139, 17309–17312. doi:10.1021/jacs.7b10846

Miyakawa, S., and Ferris, J. P. (2003). Sequence- and regioselectivity in the montmorillonite-catalyzed synthesis of RNA. *J. Am. Chem. Soc.* 125, 8202–8208. doi:10.1021/ja034328e

Nakagawa, S., Yamazaki, T., and Hirose, T. (2018). Molecular dissection of nuclear paraspeckles: Towards understanding the emerging world of the RNP milieu. *Open Biol.* 8, 180150. doi:10.1098/rsob.180150

Nakashima, K. K., Baaij, J. F., and Spruijt, E. (2018). Reversible generation of coacervate droplets in an enzymatic network. *Soft Matter* 14, 361–367. doi:10.1039/c7sm01897e

Nakashima, K. K., Vibhute, M. A., and Spruijt, E. (2019). Biomolecular chemistry in liquid phase separated compartments. *Front. Mol. Biosci.* 6, 21. doi:10.3389/fmolb.2019.00021

Papineau, D. (2010). Mineral environments on the earliest Earth. *Elements* 6, 25–30. doi:10.2113/gselements.6.1.25

Pontes-Buarque, M., Tessis, A. C., Bonapace, J. A. P., Monte, M. B. M., Souza-Barros, F. D., and Vieyra, A. (2000). Surface charges and interfaces: Implications for mineral roles in prebiotic chemistry. *An. Acad. Bras. Ciênc.* 72, 317–322. doi:10.1590/s0001-37652000000300005

Poudyal, R. R., Guth-Metzler, R. M., Veenis, A. J., Frankel, E. A., Keating, C. D., and Bevilacqua, P. C. (2019). Template-directed RNA polymerization and enhanced ribozyme catalysis inside membraneless compartments formed by coacervates. *Nat. Commun.* 10, 490. doi:10.1038/s41467-019-08353-4

Rumyantsev, A. M., Jackson, N. E., and de Pablo, J. J. (2021). Polyelectrolyte complex coacervates: Recent developments and new frontiers. *Annu. Rev. Condens. Matter Phys.* 12, 155–176. doi:10.1146/annurev-conmatphys-042020-113457

Saha, S., Weber, C. A., Nousch, M., Adame-Arana, O., Hoege, C., Hein, M. Y., et al. (2016). Polar positioning of phase-separated liquid compartments in cells regulated by an mRNA competition mechanism. *Cell* 166, 1572–1584.e16. doi:10.1016/j.cell.2016.08.006

Sahai, N., Kaddour, H., and Dalai, P. (2016). The transition from geochemistry to biogeochemistry. *Elements* 12, 389–394. doi:10.2113/gselements.12.6.389

Sand, K. K., and Jelavić, S. (2018). Mineral facilitated horizontal gene transfer: A new principle for evolution of life? *Front. Microbiol.* 9, 2217. doi:10.3389/fmicb.2018.02217

Sawyer, I. A., Sturgill, D., and Dundr, M. (2019). Membraneless nuclear organelles and the search for phases within phases. *Wiley Interdiscip. Rev. RNA* 10, e1514. doi:10.1002/wrna.1514

Sing, C. E., and Perry, S. L. (2020). Recent progress in the science of complex coacervation. *Soft Matter* 16, 2885–2914. doi:10.1039/D0SM00001A

Sowerby, S. J., Cohn, C. A., Heckl, W. M., and Holm, N. G. (2001). Differential adsorption of nucleic acid bases: Relevance to the origin of life. *Proc. Natl. Acad. Sci. U. S. A.* 98, 820–822. doi:10.1073/pnas.98.3.820

Spoelstra, W. K., Sluis, E., Dogterom, M., and Reese, L. (2019). Nonspherical coacervate shapes in an enzyme-driven active system. *Langmuir* 36, 1956–1964. doi:10.1021/acs.langmuir.9b02719

Sverjensky, D. A., and Fukushi, K. (2006). Anion adsorption on oxide surfaces: Inclusion of the water dipole in modeling the electrostatics of ligand exchange. *Environ. Sci. Technol.* 40, 263–271. doi:10.1021/es051521v

Sverjensky, D. A. (2005). Prediction of surface charge on oxides in salt solutions: Revisions for 1:1 (M^+L^-) electrolytes. *Geochim. Cosmochim. Acta* 69, 225–257. doi:10.1016/j.gca.2004.05.040

Tang, T. Y. D., Hak, C. R. C., Thompson, A. J., Kuimova, M. K., Williams, D. S., Perriman, A. W., et al. (2014). Fatty acid membrane assembly on coacervate microdroplets as a step towards a hybrid protocell model. *Nat. Chem.* 6, 527–533. doi:10.1038/nchem.1921

Turgeon, S. L., Schmitt, C., and Sanchez, C. (2007). Protein–polysaccharide complexes and coacervates. *Curr. Opin. Colloid Interface Sci.* 12, 166–178. doi:10.1016/j.cocis.2007.07.007

van Haren, M. H., Nakashima, K. K., and Spruijt, E. (2021). Coacervate-based protocells: Integration of life-like properties in a droplet. *J. Syst. Chem.* 8, 107–120.

Venturoli, D., and Rippe, B. (2005). Ficoll and dextran vs. globular proteins as probes for testing glomerular permselectivity: Effects of molecular size, shape, charge, and deformability. *Am. J. Physiology-Renal Physiology* 288, F605–F613. doi:10.1152/ajprenal.00171.2004

Wächtershäuser, G. (1992). Groundworks for an evolutionary biochemistry: The iron-sulphur world. *Prog. Biophys. Mol. Biol.* 58, 85–201. doi:10.1016/0079-6107(92)90022-X

Wächtershäuser, G. (2007). On the chemistry and evolution of the pioneer organism. *Chem. Biodivers.* 4, 584–602. doi:10.1002/cbdv.200790052

Wang, M., and Wang, Y. (2014). Development of surfactant coacervation in aqueous solution. *Soft Matter* 10, 7909–7919. doi:10.1039/c4sm01386g

Williams, D. S., Koga, S., Hak, C. R. C., Majrekar, A., Patil, A. J., Perriman, A. W., et al. (2012). Polymer/nucleotide droplets as bio-inspired functional micro-compartments. *Soft Matter* 8, 6004. doi:10.1039/c2sm25184a

Wilson, L., Matsudaira, P. T., Jena, B. P., and Horber, J. H. (2002). *Atomic force microscopy in cell biology*. Cambridge, MA, USA: Academic Press.

Xu, J., Sahai, N., Eggleston, C. M., and Schoonen, M. A. (2013). Reactive oxygen species at the oxide/water interface: Formation mechanisms and implications for prebiotic chemistry and the origin of life. *Earth Planet. Sci. Lett.* 363, 156–167. doi:10.1016/j.epsl.2012.12.008

Yewdall, N. A., André, A. A. M., Lu, T., and Spruijt, E. (2021). Coacervates as models of membraneless organelles. *Curr. Opin. Colloid Interface Sci.* 52, 101416. doi:10.1016/j.cocis.2020.101416

Zaia, D. (2004). A review of adsorption of amino acids on minerals: Was it important for origin of life? *Amino acids* 27, 113–118. doi:10.1007/s00726-004-0106-4

Zhao, W., and Wang, Y. (2017). Coacervation with surfactants: From single-chain surfactants to gemini surfactants. *Adv. Colloid Interface Sci.* 239, 199–212. doi:10.1016/j.cis.2016.04.005

Zhu, M., Souillac, P. O., Ionescu-Zanetti, C., Carter, S. A., and Fink, A. L. (2002). Surface-catalyzed amyloid fibril formation. *J. Biol. Chem.* 277, 50914–50922. doi:10.1074/jbc.m207225200

Zwicker, D., Seyboldt, R., Weber, C. A., Hyman, A. A., and Jülicher, F. (2016). Growth and division of active droplets: A model for protocells. *Nat. Phys.* 13, 408–413. doi:10.1038/nphys3984